Hinode Observations of the Onset Stage of a Solar Filament Eruption

Alphonse C. STERLING[1,2], Ronald L. MOORE[1], Thomas E. BERGER[3], Monica BOBRA[4], John M. DAVIS[1], Patricia JIBBEN[4], R. KANO[5], Loraine LUNDQUIST[4], D. MYERS[6], N. NARUKAGE[2], T. SAKAO[2], K. SHIBASAKI[7], R. SHINE[3], T. TARBELL[3], and Mark WEBER[4]

[1]*NASA/Marshall Space Flight Center, VP62/Space Science Office, Huntsville, AL 35805, USA*
asterling@spd.aas.org

[2]*JAXA/Institute of Space and Astronautical Science, Hinode Group, 3-1-1 Yoshinodai, Sagamihara, Kanagawa 229-8510, Japan*

[3]*Lockheed Palo Alto Research Laboratory, Bldg 252, 3251 Hanover Street, Palo Alto, CA 94304, USA*

[4]*Harvard-Smithsonian Center for Astrophysics, 60 Garden Street, MS-58, Cambridge MA 02138, USA*

[5]*National Astronomical Observatory, Mitaka, Tokyo 181, Japan*

[6]*Adnet Systems, Inc., 164 Rollins Avenue, Suite 303, Rockville, MD 20852, USA*

[7]*Nobeyama Radio Observatory, Minamimaki, Minamisakun, Nagano 384-1305, Japan*

(Received 2007 June 0; accepted)

Abstract

We use *Hinode* X-Ray Telescope (XRT) and Solar Optical Telescope (SOT) filtergraph (FG) Stokes-V magnetogram observations, to study the early onset of a solar eruption that includes an erupting filament that we observe in *TRACE* EUV images. The filament undergoes a slow rise for at least 20 min prior to its fast eruption and strong soft X-ray flaring; such slow rises have been previously reported, and the new *Hinode* data elucidate the physical processes occurring during this period. XRT images show that during the slow-rise phase, a soft X-ray (SXR) sigmoid forms from apparent reconnection low in the sheared core field traced by the filament, and there is a low-level intensity peak in both EUV and SXRs during the slow rise. MDI and SOT FG/V magnetograms show that the pre-eruption filament is along a neutral line between opposing-polarity enhanced network cells, and the SOT magnetograms show that these opposing fields are flowing together and canceling for at least six hours prior to eruption. From the MDI data we measure the canceling network fields to be ~ 40 G, and we estimate that $\sim 10^{19}$ Mx of flux canceled during the five hours prior to eruption; this is only $\sim 5\%$ of the total flux spanned by the eruption and flare, but apparently its tether-cutting cancelation was enough to destabilize the sigmoid field holding the filament and resulted in that field's eruption.

Key words: Sun: flares — Sun: filaments — Sun: UV radiation — Sun: X-rays, gamma rays

1. Introduction

One of the major unsolved issues of solar physics is the cause of the onset of solar eruptions. These eruptions involve magnetic regions on the Sun of various size scales, and lead to solar flares and coronal mass ejections (CMEs). In recent years the importance of CMEs in particular has become better appreciated, as their role in Space Weather and its affects on the Earth have become more clear. Such concerns have deepened our desire to understand the cause of solar eruptions, and eventually how to predict them. The *Hinode* satellite, launched in September 2006, contains an array of powerful solar instruments that will help us better understand solar eruptions and their cause. Here we present an example of a solar eruption observed by *Hinode* on 2007 March 2. We use the *Hinode* data in combination with those from the *TRACE* and *SOHO* missions to study the processes leading up to this eruption.

Eruptions involving filaments are instructive, since the filament can act as a tracer of the otherwise-invisible coronal field, and in particular motions of the filament just prior to eruption indicate how the field evolves when it is on the verge of exploding. Sometime prior to eruption the filament typically shows activity intimating possible impending eruption (Roy & Tang 1975; Rust 1976), and the filament also often begins a relatively slow rise ("slow rise phase") prior to eruption (e.g., Tandberg-Hanssen, Martin, & Hansen 1980; Kahler et al. 1988; Feynman & Ruzmaikin 2004). For quiet region events, the pre-eruption slow rise phase can last several hours (Sterling & Moore 2004; Sterling, Harra, & Moore 2007), but it can be much shorter, ~ 10 min, for active-region eruptions (Sterling & Moore 2005; Williams et al. 2005). The 2007 March 2 event occurred in an active region, and accordingly the pre-eruption evolution was relatively quick. *Hinode* and *TRACE*, however, have sufficient time and spatial resolution to follow the pre-eruption dynamics. Here we present observations of the filament from *TRACE*, and the soft X-ray (SXR) and detailed magnetic field evolution from *Hinode*. As the *Hinode* magnetic data available for this event are not yet calibrated, we also use co-temporal, but spatially and temporally more coarse magnetic field data from the the Michelson Doppler Imager (MDI) magnetograph on the *SOHO* spacecraft.

2. Instrumentation and Data

Overall, the eruption itself was rather weak in SXRs, peaking at a *GOES* class B2.5 level on 2007 March 2 at 05:29 UT, with the *GOES* data showing substantial enhancements from about 05:02 UT, and the event was located at about $300''$ W of disk center near the equator. The filament that erupts is visible in absorption in the EUV images from *TRACE*. At least portions of it are disturbed from the time of our earliest *TRACE* images at 04:28 UT, and it undergoes a slow rise prior to erupting, as discussed below (§3.3, and Fig. 3).

The *Hinode* satellite (Kosugi et al. 2007) contains three instruments: the Solar Optical Telescope, SOT (Tsuneta et al. 2007), the X-Ray Telescope, XRT (Sakao et al. 2007), and the EUV Imaging Spectrometer, EIS (Culhane et al. 2007); here we will use data from the first two of these.

From SOT we will use magnetograms constructed from the SOT filtergraph (FG) set to the magnetically-sensitive 6302 Å line. SOT was observing the I- and V-Stokes components in this line, and we use the V-Stokes data, which represent the line-of-sight magnetic field. Each original frame is 2048×1024 pixels, with a pixel size of $0.16''$. We use 21 frames between 22:20 UT on March 1 and 04:54 UT on March 2, with images nominally every 7 min, but with a gap between 22:55 UT and 03:16 UT, when data were not available.

From XRT we use images taken with its "Ti-poly" and "thick Al" filters, both of which have broad temperature response functions with peak temperature responses of several MK. Response at lower temperatures, however, is different, with Ti-poly sensitive to plasmas cooler than 1 MK, while the thick Al becomes substantially responsive to plasmas of about 2 MK and hotter. Our basic data set consists of 48 512×512-pixel images between 04:01 UT and 05:47 UT on March 2, with a typical cadence of 2 min and a pixel size of $1.032''$. This time period begins before the primary pre-eruption SXR emissions start, and continues past the time of peak flare intensity.

We have EUV data of the eruption from *TRACE* (Handy et al. 1998), specifically from its 171 Å filter, which has a peak response at about 1 MK. We use images from the start of the *TRACE* observations of this region on March 2 from 04:28 UT to 06:27 UT, with a typical cadence of 1 min and a pixel size of $0.5''$. We also use full-disk magnetograms from the MDI (Scherrer et al. 1995), which have $2''$ pixels; for the time of this event these images were taken only once about every 5 hours. Despite their lower cadence and lower spatial resolution compared to SOT, we use these MDI magnetograms because they are calibrated, while the SOT magnetograms have yet to be calibrated. In addition, the field of view of the SOT magnetogram is restricted and does not cover the entire filament, while we can select out subimages from MDI that cover the whole region of interest.

Videos 1, 2, and 3 respectively are constructed from the *TRACE*, XRT, and SOT FG/V images.

We aligned the various data sets as follows. Since the instrument pointing parameters are well understood for *TRACE* and *SOHO*, we can overlay *TRACE* EUV images onto MDI magnetograms accurately. We can align the SOT magnetograms with the MDI magnetograms by comparing frames from similar times. We then initially aligned XRT images onto SOT magnetograms, and subsequently onto MDI magnetograms, using preliminary alignment information among the three *Hinode* instruments derived within the *Hinode* team (H. Hara 2007, private correspondence; N. Narukage 2007, private correspondence). We then adjusted the alignment by eye, e.g., matching bright features in XRT with stronger magnetic elements. Based on the matching of such features across the field of view that we use, we estimate our final alignment to be accurate to $< 10''$.

3. Observations and Analysis

3.1. EUV Evolution

Figure 1 shows *TRACE* frames of the erupting region, with an MDI magnetogram overlaid. Prior to eruption the filament is activated and moves upward, with the filament obviously having

changed position between Figures (1a) and (1b) (see §3.3). A new EUV loop (red arrow in Fig. 2b) brightens from its westernmost-side base beginning at 04:37 UT, and the illumination propagates along the loop, reaching the apex at about 4:42 UT and the opposite (East) base at about 4:51 UT. Over the first 5 minutes we estimate that this brightening travels about 50,000 km from the West base to the apex, giving a velocity of ~ 170 km s^{-1}, to about a factor of two. In Figure 1c the filament is starting violent motions coinciding with the onset of flare brightenings.

3.2. SXR Evolution

Figure 2 shows images from XRT overlaid onto the same MDI magnetogram as that in Figure 1, and panels (a), (b), and (d) of Figure 2 roughly correspond respectively to panels (a), (b), and (c) of Figure 1. Figure 2a is prior to the start of the obvious pre-eruption brightenings. Figure 2b, about 20 min prior to the main flare, shows a sigmoid loop developing. From movies made from these XRT images (Video 2), this loop appears to be developing near the locations indicated by the white and black arrows in the figure. This loop begins with what appears as an outflow from this location between images at 4:28 UT and 4:30 UT, and by the next image at 4:32 UT the entire northern "elbow" of the sigmoid (Moore et al. 2001) is discernable. By 4:45 UT it is a detached sigmoid loop, with the north elbow indicated by the red arrow in Figure 2b. This sigmoid loop continues to expand outward, and appears to arch out to a more semicircular shape by the time of Figures 2d and 2e, although much of this erupting sigmoid is obscured by saturation in the XRT images. From this time the arched sigmoid structure is escaping from the Sun as the field apparently opens up, and is beyond the frame's field of view in Figure 2f. On average, between images at 5:12 UT and 5:21 UT the outward-moving front (red arrows in Figs. 2d and 2e) has velocity of about 100 km s^{-1}, in the plane normal to the line-of-sight. This could, however, correspond to the accelerating structure seen in SXRs by Alexander, Metcalf, & Nitta (2002). At earlier times it appears that similar but fainter sigmoid loops were ejected from the same location, suggesting formation by sequential episodes of reconnection in the middle of the sheared core field holding the filament.

At the base of the erupting location, the footpoints of the brightest SXR loops during the very early eruption phase (Fig. 2d) are rooted in strong magnetic elements near the location where the sigmoid forms (white and black arrows in Fig. 2b), but later in the flare development, the situation changes so that the brightest loops have footpoints rooted farther away from the core (white arrows in Fig. 2e). This change may come about because of the attraction of the very strong field near the sunspot in the southwest (near coordinates ($330''$,$20''$)) caused the feet of the reconnected field to jump to that strong field, or because the initial sigmoid eruption excited loops in a secondary episode that had pre-existing connections to the strong sunspot field. In the north of Figure 2f there is additional strong SXR emission that may be due to field that may have opened (or partially opened) up due to complex secondary processes (such as ejection of a larger, overlying magnetic structure, e.g. Moore & Sterling 2007), although a comprehensive analysis of these features is beyond the scope of the present investigation.

3.3. Filament Motions

Figure 3 shows the trajectory, projected on the solar disk, of a portion of the filament as a function of time. It is undergoing a "slow-rise phase" from at least the time of the start of the *TRACE* observations, it undergoes a disturbance at about 04:45 UT, and has a "fast-rise phase" starting between 05:05 UT and 05:12 UT.

We chose to follow the filament along the Figure 1a fiducial, since along it we can track the pre-eruption motions relatively consistently; the orientation of the fiducial was selected to follow the approximate direction in which the filament is ejected out of the field of view. Actual motions of the filament, however, are complex, with different parts of the filament having different behavior (see video 1). Thus, although the trajectory if Figure 3 is indicative of the entire filament's motion, detailed trajectories will differ for different parts of the filament. Our main emphasis is that there is a slow evolution (slow-rise phase) prior the the ejection (fast-rise phase). Also, it is difficult to sort out which of the filament's motions are in the vertical direction. In fact, the filament undergoes a counter-clockwise twist between about 5:00 and 5:15 UT, and this is suggestive of a kink instability (similar to an event studied by Williams et al. 2005), as discussed further below. During the slow rise phase, there is a burst in intensity in both the *TRACE* EUV images and in the XRT SXR images, in the lightcurves from, respectively, the location of the new EUV loop of Figure 1b and the location where the sigmoid forms in Figures 2a—2c; this burst disturbs the filament trajectory. Later, there is a bright flaring apparent in *TRACE* from 05:10 UT, while the XRT intensity is saturated due to flaring from 05:02:37 UT.

3.4. Magnetic Field Behavior

Both the west end (the source of the propagating emission) of the new loop of Figure 1b and the point of formation of the sigmoid of Figure 2b are at approximately the same location, viz. that indicated by the white and black arrows in Figure 2b. From the MDI magnetograms in Figures 1 and 2, this location is near a site of merging opposite-polarity magnetic elements along the neutral line of the pre-erupting filament. To gain clues to the source of these features, the likely ultimate source of the eruption, we investigate more closely the behavior of the magnetic field around this location with SOT.

Figure 4 shows SOT FG/V images around the erupting region. One can identify common features in Figure 4a with the MDI magnetograms in Figures 2d—2f, with the sunspot at the right edge near $20''$ N. East of the spot are two partially-complete positive enhanced-network cells, and the two furthest east of these flux clumps butt up against part of an irregularly-shaped negative-polarity enhanced-network cell; the box in Figure 4a is centered on this colliding-positive-negative location. Again comparing with Figure 1, we see that it is this location that contains the neutral line upon which the filament existed prior to eruption, and from where the eruption emanated.

Figures 4b—4d show the evolution over time of the field of the region of the white box in Figure 4a. As mentioned in §2, there is a time gap in these data, and it occurs between the images in

Figures 4b and 4c. A movie made from these SOT images (Video 3) however indicates that over this time gap the negative and positive regions flowed into each other. For example, in Figure 4b both the large positive clump of field near ($218''$,$26''$) and the negative clump near ($205''$,$40''$) are not apparent in Figure 4c; because of the overall flow pattern apparent in the movie, we assume that these clumps have each largely canceled with respective opposing polarities. This flow continues, and more flux has canceled by the time of Figure 4d (which is identical to the time of Fig. 4a).

We would like to determine the amount of flux-change with time in the region around where the eruption appears to begin. We select the black box in Figure 4d (also shown in Fig. 4a) for this estimate. We do not, however, use the SOT data for this purpose, because as of the time of this writing those data are not yet calibrated. Instead, we measure the flux in the same location in the MDI images. We have three appropriate images, at 19:15 UT on 2007 March 1, and at 00:03 UT and 04:51 UT on 2007 March 2; in each case we have selected a box close to the black box of Figure 4, but at each time we have adjusted the boundary slightly so that each box covers the same gross features. We find unsigned magnetic flux values for these three times to be, respectively, 3.0×10^{19} Mx, 3.4×10^{19} Mx, and 1.0×10^{19} Mx. Thus, there is a substantial drop in the unsigned magnetic flux between 00 UT and the time of the eruption near 5 UT, and this is consistent with the flux cancelation shown by the SOT FG/V magnetograms. (Our MDI flux values do not include an adjustment factor obtained by Berger & Lites 2003, which would increase the stated values by about a factor of about 1.5.) From following some of the seemingly most rapid of the elements converging toward the neutral line between Figures 4b and 4c, we deduce converging velocities of 0.45 ± 0.15 km s^{-1}, where the error is from uncertainty in identification of identical converging clumps of magnetic elements in the two frames.

4. Interpretation and Discussion

We can summarize our observations as follows. Over 20 min prior to the onset of strong SXR flare emission at 5:02 UT on 2007 March 2, a sigmoid was growing via reconnection at the location of the white and black arrows in Figure 2b, with these arrows showing the roots of the "lower reconnection product," where the sigmoid is the "upper reconnection product." Also during this pre-flare period there were slow motions of a filament visible in EUV. A new EUV loop appeared during the slow-rise; to within our alignment accuracy, the EUV loop is a strand of the north portion of the XRT sigmoid. Thus both the north elbow of the sigmoid and EUV loop arch over the filament. Both the EUV loop and the site of the sigmoid formation undergo a burst in intensity, disturbing the filament's slow rise, near 04:45 UT. Sterling & Moore (2005) and Sterling, Harra, & Moore (2007) have seen similar SXR intensity brightenings prior to the main flare that were related to the slow-rise phase of filaments, and this could be the flare precursor brightening discussed by Harrison (1986), which he suggested was related to CME onset. SOT and MDI data show that the location where the sigmoid forms and from where the EUV-loop emissions emanate are on a neutral line where opposite-polarity magnetic flux convergence had been occurring since at least 22 UT on March 1.

Figure 5 shows our interpretation of these observations. The green and magenta field lines are poised to reconnect, forming the low-lying black loop and an out-moving sigmoid loop. There would be other loops similar to the green and magenta loops that would subsequently reconnect, although clumps of magnetic field in the photosphere would tend to make the reconnection episodic; this would account for the fainter-illumination sigmoid fields that we see in the XRT images prior to production of the bright sigmoid of Figures 2b and 2c. Reconnection of these fields reduces field restraining the filament field, and results in the slow rise of the filament; Moore & Roumeliotis (1992) discussed the slow start to eruptions by such processes, which they called "slowly driven tether cutting." Sterling, Harra, & Moore (2007) present a slightly different example where "tether weakening" reconnection appears to be occurring. In both cases, each reconnection episode results in a further rise of the filament.

Key to the reconnections at the crossing point of the Figure 5 green and magenta field lines, is the converging of the photospheric magnetic field as revealed by the SOT FG/V data. Cancelation of this flux at the neutral line leads to reconnection at the green-magenta field crossing point (which is near location of the white arrow in Fig. 2b), producing the short lower reconnection loop and the rising filament-holding SXR sigmoid, the activation and slow rise of the filament, and eventually to disruption of the whole field system resulting in the fast filament rise in the violent eruption.

From the fluxes derived from the MDI data in the previous Section, we can make an estimate of the strength of the field above the noise level (which we take as 10 G) in the region of the black box in Figures 4a and 4d, and we derive this strength, $B,$ to be about 40 G. (The 1.5 factor of Berger & Lites 2003 would make this 60 G.) Thus the fields are not very strong. Moreover, we measure that the entire immediate erupting and flaring region, which we estimate to span $150''$—$300''$ in x and $0''$—$150''$ in $y,$ (see e.g. Fig. 2, however this ignores possible secondary eruptions covering a larger area), to have flux $\sim 5 \times 10^{20}$ Mx, and so the a flux change of $\sim 5\%$ over the last 5 hours prior to eruption is enough to begin the release of energy contained in the pre-existing sheared field by some mechanism, such as an instability, leading to the eruption. van Ballegooijen & Martens (1989) suggest that long-term flux cancelation can result in filament-supporting flux-tube geometries, and to the eventual destabilization and eruption of the filament; this could be what is occurring here.

The erupting sigmoid loop we see in Figure 2 is similar to the type described by Rust & Kumar (1996) and Pevtsov, Canfield, & Zirin (1996), where the sigmoid loop is made by the reconnection of the crossed arms of the elbows in the onset of eruption, in contrast to the longer-lasting sigmoid-shaped active regions discussed by, e.g., Canfield, Hudson, & McKenzie (1999) and Sterling et al. (2000). Both types, however, are a consequence of the sheared nature of the magnetic field in erupting regions and many active regions. Moore et al. (2001) also saw a developing sigmoid of the type we observe here (see their Fig. 5).

Rust & Kumar (1996) also discuss the kink-mode instability in the context of eruptions. Our filament undergoes writhing near the onset of the fast-rise phase, and so a combination of tether-weakening reconnection, along with tether-cutting reconnection and the kink instability could be the

release mechanism for the fast-rise phase of the eruption; this is similar to the conclusion reached by Williams et al. (2005) for a filament eruption they observed.

We thank the anonymous referee for useful comments. A.C.S. and R.L.M. were supported by funding from NASA's Office of Space Science through the Solar Physics Supporting Research and Technology Program and the Sun-Earth Connection Guest Investigator Program. *Hinode* is a Japanese mission developed and launched by ISAS/JAXA, collaborating with NAOJ as a domestic partner, NASA and STFC (UK) as international partners. Scientific operation of the Hinode mission is conducted by the Hinode science team organized at ISAS/JAXA. This team mainly consists of scientists from institutes in the partner countries. Support for the post-launch operation is provided by JAXA and NAOJ (Japan), STFC (U.K.), NASA, ESA, and NSC (Norway). We also acknowledge the invaluable contribution made to the *Hinode* project by our colleague and friend, Dr. Takeo Kosugi, who sadly passed away shortly after *Hinode*'s launch.

References

Alexander, D., Metcalf, T. R., & Nitta, N. V. 2002, Geophys. Res. Lett., 29(10), 1403

Berger, T. E., & Lites, B. W. 2003, Sol. Phys., 213, 213

Canfield, R. C., Hudson, H. S., & McKenzie, D. E. 1999, Geophys. Res. Lett., 26, 627

Culhane, J. L., et al., Sol. Phys., submitted.

Feynman, J., & Ruzmaikin, A. 2004, Sol. Phys., 219, 301

Handy, B. N., Bruner, M. E., Tarbell, T. D., Title, A. M., Wolfson, C. J., Laforge, M. J., & Oliver, J. J. 1998, Sol. Phys., 187, 29

Harrison, R. A. 1986, A&A, 162, 283

Kahler, S. W., Moore, R. L., Kane, S. R., & Zirin, H. 1988, Sol. Phys., 328, 824

Kosugi, T., et al., Sol. Phys., submitted.

Moore, R. L., & Roumeliotis, G. 1992, in Eruptive Solar Flares, ed. Z. Svestka, B. V. Jackson, & M. E. Machado (Berlin: Springer), 69

Moore, R. L., Sterling, A. C., Hudson, H. S., & Lemen, J. R. 2001, 552, 833

Moore, R. L., & Sterling, A. C. 2007, ApJ, 661, 543

Pevtsov, A. A., Canfield, R. C., & Zirin, H. 1996, ApJ, 473, 533

Roy, J.-R., & Tang, F. 1975, Sol. Phys., 42, 425.

Rust, D. M. 1976, Sol. Phys., 47, 21

Rust, D. M., & Kumar, A. 1996, ApJ, 464, L199

Sakao., T. et al. 2007, Sol. Phys., submitted.

Scherrer, P. H., et al. 1995, Sol. Phys., 162, 129

Sterling, A. C., Hudson, H. S., Thompson, B. J., & Zarro, D. M. 2000, ApJ, 532, 628

Sterling, A. C., & Moore, R. L. 2004, ApJ, 602, 1024

Sterling, A. C., & Moore, R. L. 2005, ApJ, 630, 1148

Sterling, A. C., Harra, L. K., & Moore, R. L. 2007, ApJ, in press

Tandberg-Hanssen, E., Martin, S. F., & Hansen, R. T. 1980, Sol. Phys., 65, 357

Tsuneta, S., et al. 2007, Sol. Phys., submitted.
van Ballegooijen, A. A., & Martens, P. C. H. 1989, ApJ, 343, 971
Williams, D. R., Torok, T., Demoulin, P., van Driel-Gesztelyi, L., & Kliem, B. 2005, ApJL, 628, L163

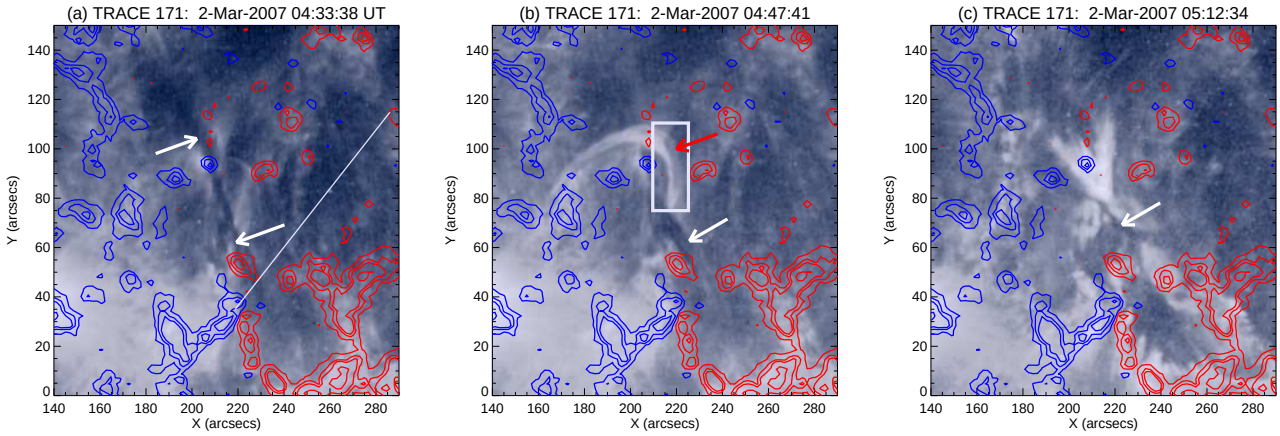

Fig. 1. *TRACE* 171Å images of the erupting filament (white arrows), and a new loop that brightens during the pre-eruption phase (red arrow in b). Red and blue contours are respectively positive and negative polarities from an MDI magnetogram from 4:51 UT on 2007 Mar 2; contour levels are 15, 50, 100, and 300 G. Panels (a) and (b) span a pre-eruption phase when the filament is undergoing a slow rise and other motions, and panel (c) is from near the time of onset of the filament's fast eruption. In (a) the white fiducial line is used to determine the filament height as a function of time in Fig. 3, and the box in (b) is for for generating the lightcurve of Fig. 3. North is up and East to the left in these and all images in this paper. Video 1 is a movie of the *TRACE* images.

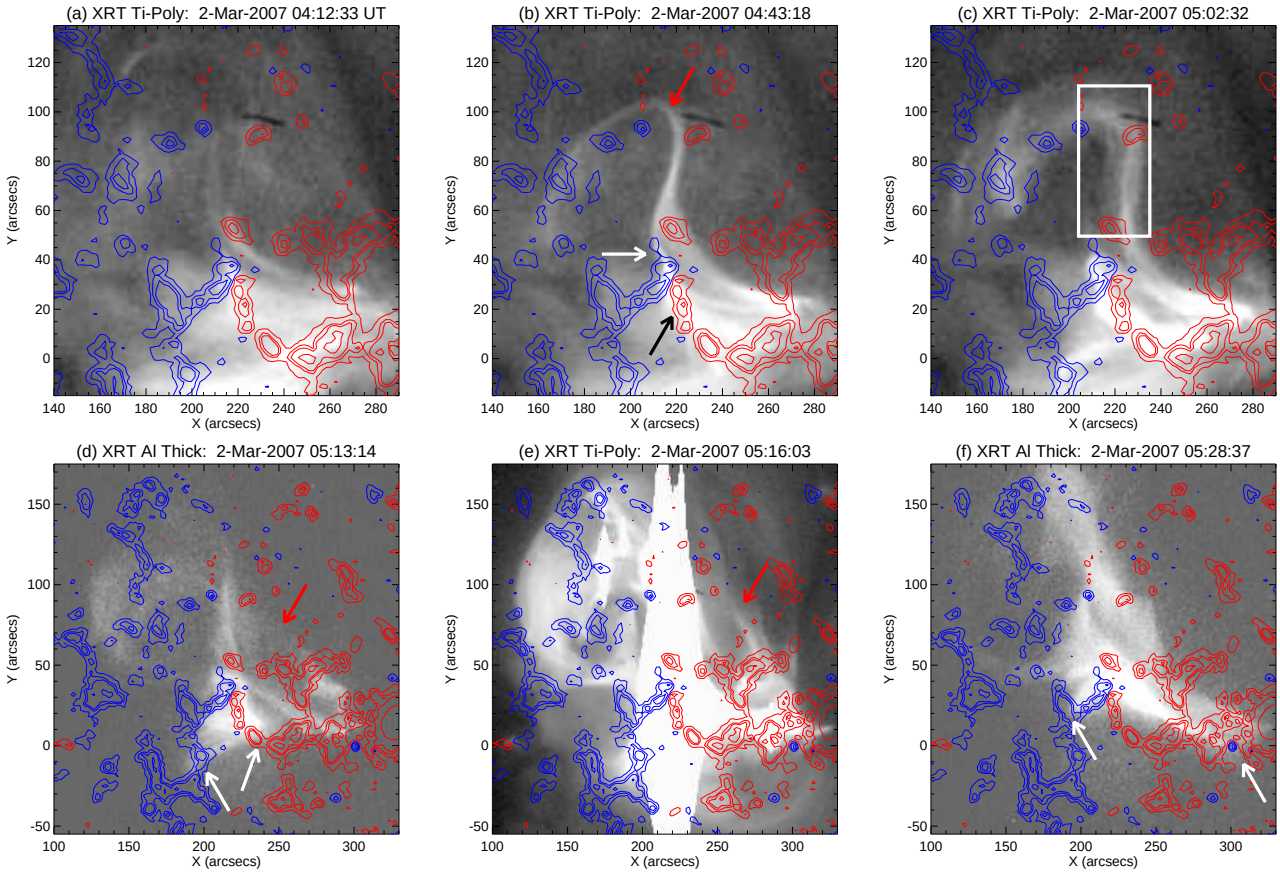

Fig. 2. *Hinode* XRT SXR images of the erupting region, on the same MDI magnetogram contours as in Fig. 1. Panels (a)—(c) are during the pre-eruption period, (d) and (e) are from about the time of the start of the eruption and the filament's fast rise, and (f) is near the time of the flare's peak intensity. In (b), the red arrow points to the north part of a sigmoid loop, and this corresponds to the EUV loop of Fig. 1b. The white and black arrows point out the roots of the lower reconnection product, and that loop appears bright in the XRT movie. In (d) and (e) the red arrows point to the middle part of the erupting sigmoid structure. White arrows in (d) and (f) point to the footpoints of bright loop arcades, which shift between the pre-eruption period of (d) and the time near the flare peak in (f). The bright streaking in (e) is due to saturation of the XRT CCD. In (c) the boxed region is used to generate the lightcurve in Fig. 3. Video 2 is a movie of the XRT images on the scale of panels (a)—(c).

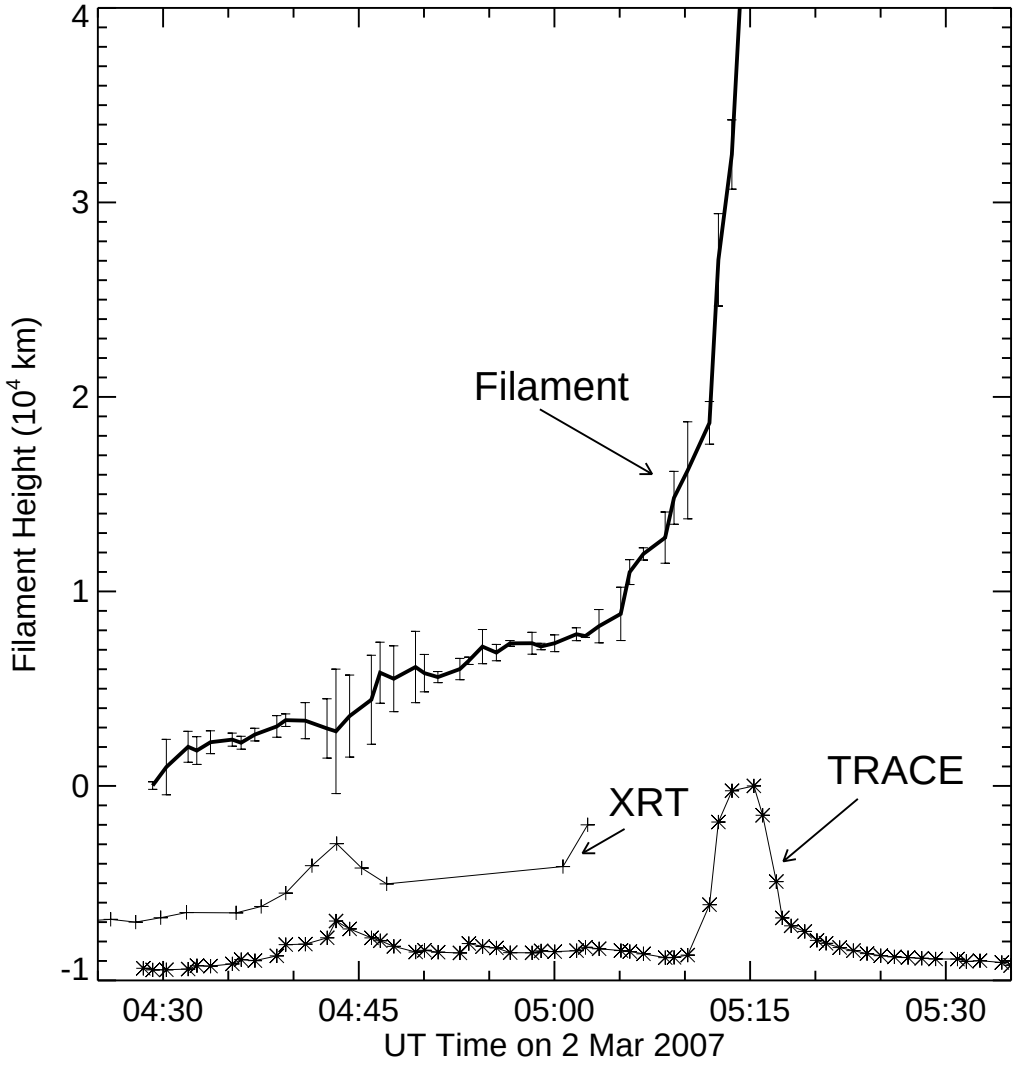

Fig. 3. Height as a function of time for a portion of the filament seen in *TRACE* images, along the fiducial of Fig. 1. Error bars are from are 1σ uncertainties from three repeated measurements of the filament positions. Also shown are lightcurves of integrated intensities (with arbitrary vertical scaling) from *TRACE* and XRT from the boxed regions in Figs 1b and 2c, respectively.

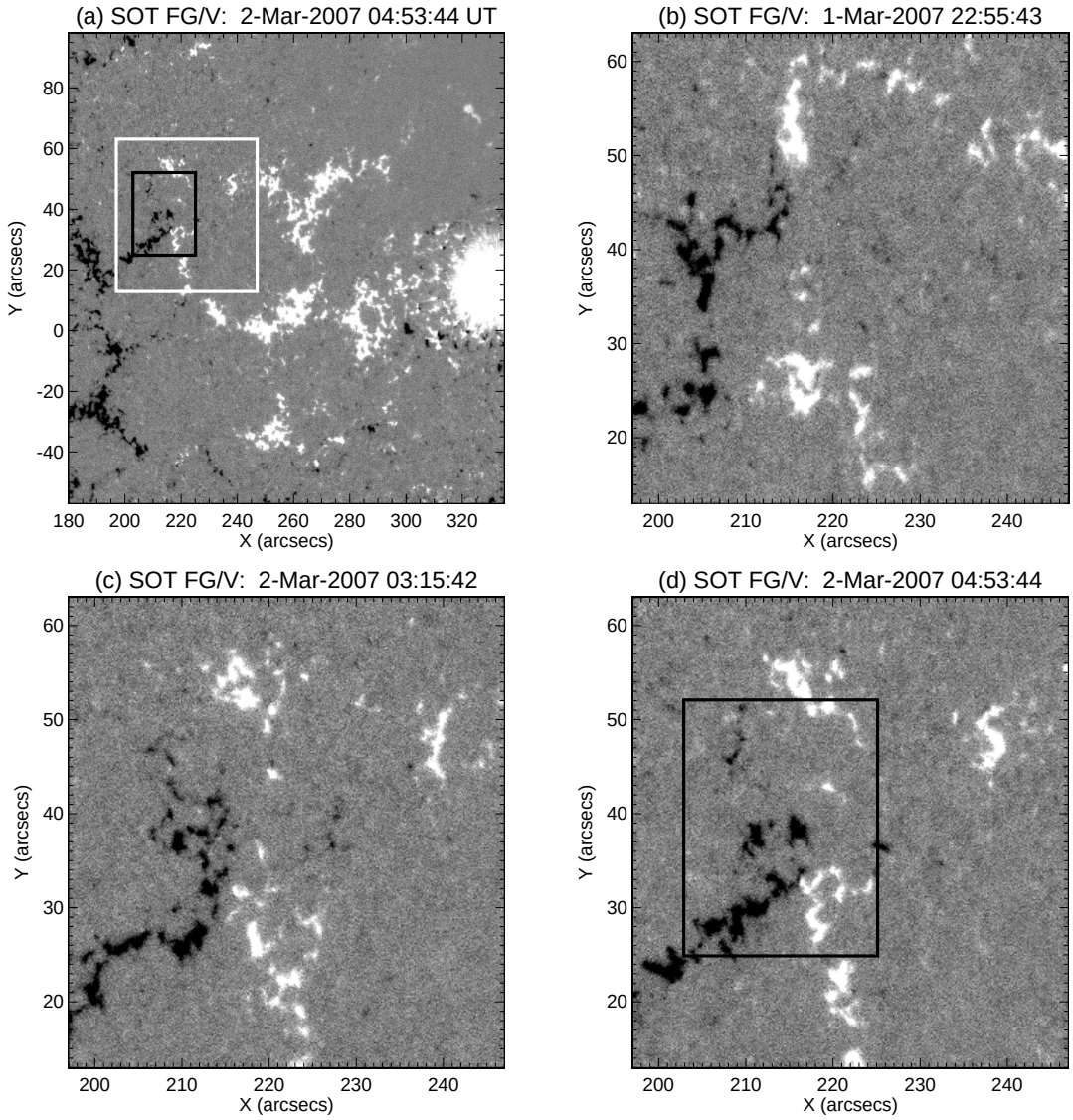

Fig. 4. SOT FG Stokes-V magnetograms of the erupting region. Comparing these with the MDI magnetogram and *TRACE* images of Fig. 1 shows the relation to the filament. Panel (a) is a context image showing a nearby sunspot, and Panels (b)—(d) show a close up of the neutral line under the erupting sigmoid, from the white box in (a), at different times. White and black show positive and negative polarities. These opposite polarities undergo flux cancelation over time, as calculations of the total unsigned polarity in the back box of (a) and d) show (see text). Video 3 is a movie of the SOT images on the scale of panel (a).

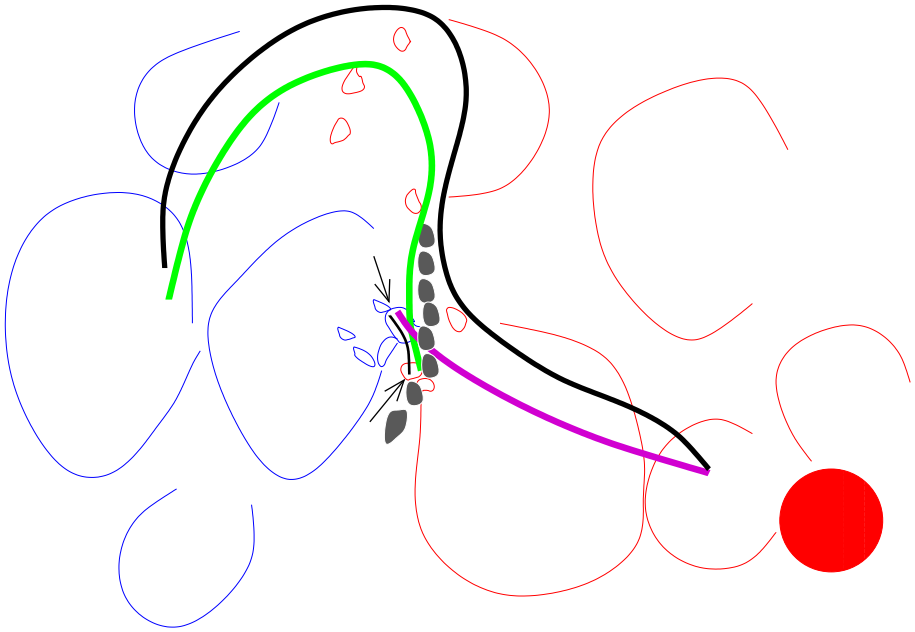

Fig. 5. Schematic interpretation of the eruption of Figs. 1—4. Red and blue contours roughly correspond to the magnetic pattern in the MDI (Figs. 1 and 2) and SOT FG/V (Fig. 4) magnetograms, the broken shaded feature represents the filament along the neutral line of the black box of Fig. 4. The green field curve represents the loop seen in EUV (Fig. 1b) in the North part of the sigmoid of Fig. 2. The magenta curve represents a field line extending from the region around the sunspot in Figs. 2d—2f. Magnetic reconnection between the the field of the green and magenta structures results in two reconnection products: the sigmoid of Fig. 2, and smaller loops that straddle the neutral line and which have footpoints indicated by the two arrows, and these correspond to the white and black arrows in Fig. 2d; both of these reconnection products are drawn as black lines in the schematic.